Journal Pre-proofs

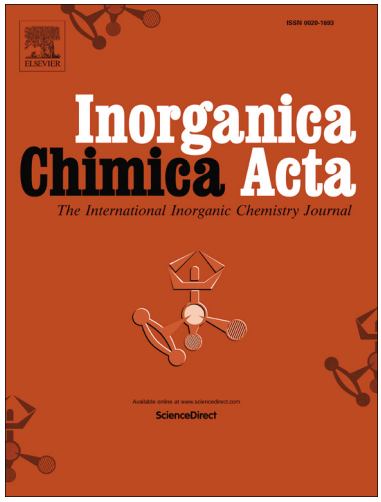

Synthesis of Novel Metal (II) Complexes Tailored from 9-Oxo-9*H*-fluorene-1-carboxylic Acid *via* Green Protocol: DNA Cleavage and Anticancer Studies

Mahantesh Kumbar, Sangamesh A. Patil, Shivakumar S. Toragalmath, Shailaja S. Jawoor, Arun Shettar

PII: S0020-1693(19)31024-2
DOI: https://doi.org/10.1016/j.ica.2019.119210
Reference: ICA 119210

To appear in: *Inorganica Chimica Acta*

Received Date: 22 July 2019
Revised Date: 29 September 2019
Accepted Date: 14 October 2019

Please cite this article as: M. Kumbar, S.A. Patil, S.S. Toragalmath, S.S. Jawoor, A. Shettar, Synthesis of Novel Metal (II) Complexes Tailored from 9-Oxo-9*H*-fluorene-1-carboxylic Acid *via* Green Protocol: DNA Cleavage and Anticancer Studies, *Inorganica Chimica Acta* (2019), doi: https://doi.org/10.1016/j.ica.2019.119210

Synthesis of Novel Metal (II) Complexes Tailored from 9-Oxo-9*H*-fluorene-1-carboxylic Acid *via* Green Protocol: DNA Cleavage and Anticancer Studies

Mahantesh Kumbar[a], Sangamesh A. Patil[a]*, Shivakumar S. Toragalmath[b], Shailaja S. Jawoor[a], Arun Shettar[c]

[a]P. G. Department of Chemistry, Karnatak University, Dharwad 580 003, Karnataka, India.

[b]K L E's, P. C. Jabin Science College, Autonomous, Vidyanagar, Hubballi 580 031, Karnataka, India.

[c]P. G. Department of Biotechnology and Microbiology, Karnatak University, Dharwad 580 003, Karnataka, India.

*Corresponding author e-mail: patil1956@rediffmail.com Contact no: +91 9986265906

Abstract

Despite being a polycyclic aromatic compound, fluorenone is not classified as carcinogenic. Some of the derivatives of fluorenone and metal complexes embedded with fluorenone based ligands exhibited challenging biological activities, including anticancer activity. The current investigation hence focuses on synthesis, characterization and anticancer activities of fluorenone based ligands and their coordinate compounds of some first row transition metals. The stoichiometry of all the synthesized metal complexes is found to be 1: 2 (metal: ligand) with the general formula $[M(L)_2]$, L = singly deprotonated ligand, whereas the geometry of all the metal complexes is found to be octahedral. The synthesized ligands and their respective metal (II) complexes were found to cleave the pBR322 DNA, during gel electrophoresis studies. The inhibition of cancer cell growth has been confirmed by fluorescence imaging techniques using DAPI as staining dye. The IC50 values of ligands and their metal (II) complexes suggest that synthesized compounds are more active towards A549 (human lung adenocarcinoma) cell line when compared with the standard drug Paclitaxel. In case of MCF-7 (human breast carcinoma) cell line, compound $Cu(L^2)_2$ is found to be more active than the standard drug Paclitaxel.

Keywords: 9-oxo-9*H*-fluorene-1-carboxylic acid, green synthesis, DNA cleavage, anticancer, cytotoxicity.

Highlights

- The manuscript describes the synthesis of two new hydrazone Schiff base ligands.
- Synthesis of metal complexes from greener protocol.
- Structure of synthesized compounds was confirmed by analytical and spectroscopic methods.
- DNA cleavage, DAPI staining and anticancer activity studies were carried out.
- Study confirms that, synthesized compounds are more active towards A549 cell line when compared to that of standard drug Paclitaxel.

1. Introduction

Cardiovascular disease and cancer are the top two medical challenges for the 21st-century scientific community, which are the serious cause of mortality worldwide [1]. Despite advances in biomedical research and technology, cancer is a growing public health issue, particularly in developed countries [2, 3]. By 2030, the global burden due to cancer incidence is expected to grow to 21.7 million [4]. The increasing incidence of cancer worldwide could be largely due to environmental factors, such as tobacco smoking, urbanization and its associated pollution, changing diet patterns and extended post-reproductive life span [5]. The cancer spreads when genetic changes interfere with the orderly process of mitosis and apoptosis. Cells start to grow uncontrollably and they may form a mass called '*tumor'*, which could be cancerous or benign. A cancerous tumor is malignant; it can grow and spread to other parts of the body whereas benign tumor can grow but will not spread [6, 7].

Current treatment includes gold standard strategies like surgical excision, chemotherapy, and radiotherapy which are adopted individually or in combination [8]. Many therapeutic agents have been isolated from animals, plants and minerals, as well as major of them, are synthesized in the laboratory. Chemotherapeutic agents like doxorubicin, paclitaxel, cabazitaxel, granisetron, docetaxel, letrozole and platinum based drugs like carboplatin, nedaplatin, oxaliplatin, lobaplatin remain as a principal mode of treating various cancers. However, most of them suffer from various side effects including fatigue, appetite loss, sore mouth, changes in taste, fever, infection, anxiety, depression, nausea and vomiting which are the prime setbacks in their clinical utility [9, 10]. In order to get rid of these disadvantages of side effects, current effort in the development of novel metallodrugs [11, 12] focused more and more on the use of transition metal complexes with unconventional and unprecedented organic ligands. Hence, the current expedition focuses on synthesizing new organic moieties with suitable donor atoms and their metal complexes, which may help better in treating vulnerable cancer. The literature survey reveals that, fluorenone being a polycyclic aromatic compound, has exhibited reasonable to challenging biological activities including anticancer properties [13, 14]. Hence, the current study focuses on synthesizing new fluorenone based hydrazone Schiff bases and their metal (II) complexes owing to their excellent biological activity and as anticancer agents. The fluorenone derivatives were identified as a histamine H3 inhibitor [15]. 1-methoxydiazofluorene can inhibit the proliferation of HeLa cells [16]. Fluorenone-carboxamide scaffolds are proved to be potent and have selective

binding properties for tetraplex DNA [17]. Structure-activity relationship for the carboxamide group present in various N-aryl-9-oxo-9*H*-fluorene-1-carboxamides have been studied and N-(2-(*1H*-pyrazol-1-yl)phenyl)-9-oxo-*9H*-fluorene carboxamide is identified as a lead compound with increased aqueous solubility, was found to retain the broad activity in the caspase activation assay and in the cell growth inhibition assay [18, 19]. The antiproliferative activity of tri- and tetraazabenzo[3,2-a]fluorene-5,6-dione derivatives is comparable with that of standard drugs Mitoxantrone and Doxorubicin [20]. In the present study, we have successfully incorporated above discussed functional groups viz., carboxamide, carboxylic acid and hydrazone Schiff base into our newly designed fluorenone based ligands and synthesized transition metal (II) complexes from these ligands and characterized thoroughly using analytical and spectroscopic techniques. The metal (II) complexes and their respective ligands were screened for their potency towards anticancer activities for A549 and MCF-7 cell lines and mode of cell death through fluorescence imaging using DAPI [4′,6-diamidino-2-phenylindole] staining method. The DNA cleavage studies were carried out with gel electrophoresis technique.

2. Experimental

2.1 Materials and Instrumentation

All the raw materials including reagents, catalysts, solvents and drying agents were of fine chemical grade and utilized as received by the vendor.

Infrared (IR) spectra of the synthesized materials were recorded in the range of 4000-550 cm^{-1} with *PerkinElmer Spectrum Two* FT-IR spectrometer. By using TMS as internal reference compound, ^{1}H and ^{13}C NMR spectra were recorded in DMSO-d_6 solvent on JEOL 400 MHz and BRUKER 400 MHz spectrometer at room temperature. Using *Thermo Quest* elemental analyzer, elemental analysis of the compounds is carried out. Electronic spectra of ligands and their metal(II) complexes were recorded on a *PerkinElmer LAMBDA 365* UV-Vis spectrophotometer in the range of 1100-200 nm. Thermal analysis of the metal complexes was carried out with an *SDT Q600 V20.9* analyzer, by increasing the temperature from RT to 1000 °C at the rate of 10 °C min^{-1}. The molar conductivity measurements were made on *ELICO CM* 180 conductivity meter with a cell constant of 1.0 after calibration with standard KCl solution at 25 °C. LC-ESI-MS spectra were recorded on *LCMS 2010A, SHIMADZU* instrument.

2.2 Synthetic Procedure

2.2.1 Procedure for the synthesis of 9-oxo-9H-fluorene-1-carboxylic acid

9-Oxo-9*H*-fluorene-1-carboxylic acid is prepared from fluoranthene using potassium dichromate as an oxidizing agent as per the protocol reported in our previous publication [21]. Yield: 99%. Color: Orange. M. P: 194-196 °C (Lit.: 196-198 °C). Scheme 1 depicts the synthetic route for 9-oxo-9*H*-fluorene-1-carboxylic acid.

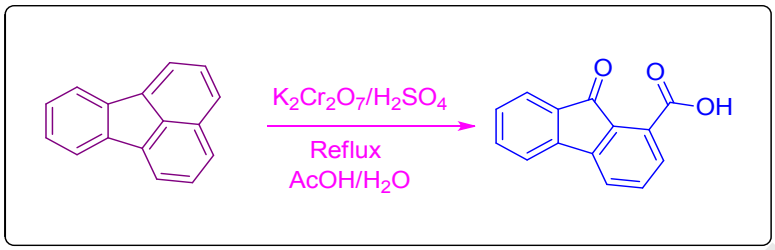

Scheme 1: Schematic for the synthesis of 9-oxo-*9H*-fluorene-1-carboxylic acid.

2.2.2 General procedure for the synthesis of hydrazone Schiff base

An equimolar mixture (2.5 g, 11.15 mmol) of 9-oxo-9*H*-fluorene-1-carboxylic acid and benzohydrazide (1.52 g, 11.15 mmol) is refluxed in methanol at 70 °C for 8 h [22]. The contents are partially soluble at RT. About 30 min of heating at 70 °C, the reaction mixture turns orange to yellow and yellow solid gets separated. The reaction is monitored by TLC in 9: 1 chloroform: methanol. The solids are filtered and washed with cold methanol and dried under *vacuo* at 40 °C. Scheme 2 represents the synthesis of hydrazone Schiff bases. Yield: LH^1: Yield: 3.55 g, 93%. Color: Yellow. LH^2: Yield: 3.60 g, 90%. Color: Yellow.

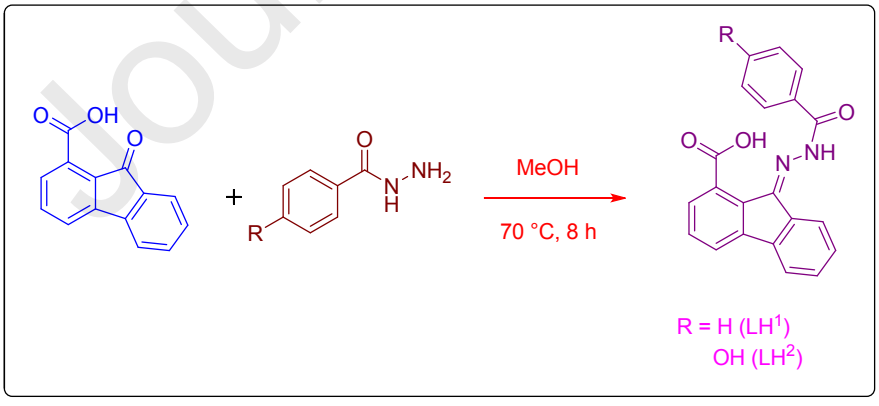

Scheme 2: Schematic for the synthesis of hydrazone Schiff base.

2.2.3 Green procedure for the synthesis of transition metal complexes

Copper complex: The copper(II) complexes are synthesized in water at room temperature. Equimolar mixtures of ligand (500 mg, 1.46 mmol), copper (II) chloride (250 mg, 1.46 mmol) and sodium acetate (120 mg, 1.46 mmol) are stirred in DI (deionized) water for 8 h at RT. The solid separated is filtered, washed with water and dried under *vacuo* at 50 °C. $Cu(L^1)_2$: Yield: 283 mg, 52%. Color: Green. $Cu(L^2)_2$: Yield: 315 mg, 58%. Color: Brown.

Nickel/Cobalt complexes: The Co(II) and Ni(II) complexes are synthesized in water under reflux conditions. Equimolar mixtures of ligand (500 mg, 1.46 mmol), metal (II) chloride ($CoCl_2.6H_2O$/$NiCl_2.6H_2O$) and sodium acetate (120 mg, 1.46 mmol) are refluxed in DI (deionized) water for 8 h. The solid separated is filtered, washed with water and dried under *vacuo* at 50 °C. Scheme 3 represents the synthesis of transition metal (II) complexes. $Co(L^1)_2$: Yield: 260 mg, 48%. Color: Yellow. $Co(L^2)_2$: Yield: 270 mg, 50%. Color: Brownish yellow. $Ni(L^1)_2$: Yield: 243 mg, 45%. Color: Yellow. $Ni(L^2)_2$: Yield: 226 mg, 42%. Color: Yellow.

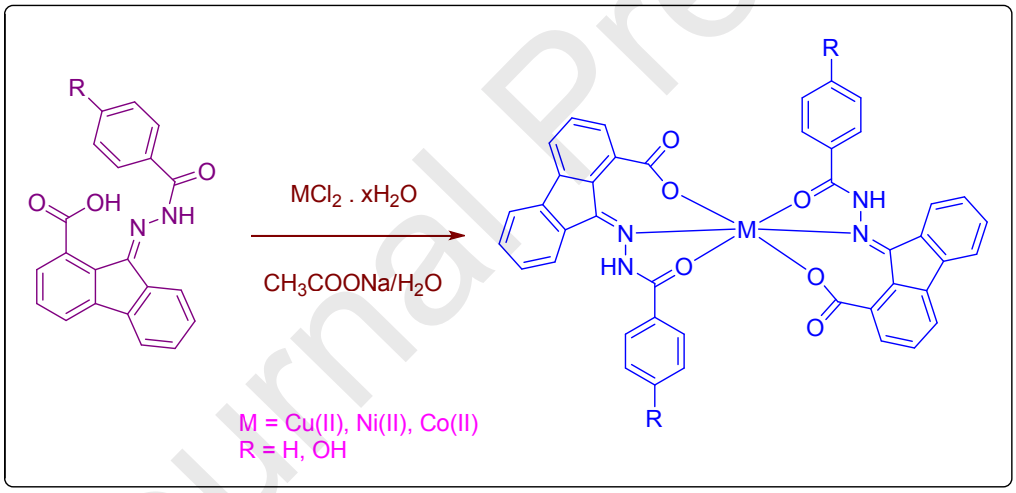

Scheme 3: Schematic for the synthesis of transition metal (II) complexes.

2.3. Bioassay Procedure

2.3.1 Cytotoxicity: MTT Cell Proliferation Assay

The cells were seeded at a density of approximately 5×10^3 cellswell^{-1} in a 96-well flat-bottom microtitre plate and maintained at 37 °C overnight in 95% humidity and 5% CO_2. Different concentrations (50, 40, 30, 20, 10, 5 μM) of samples were treated and the cells were incubated for another 48 h. The cells in well were washed twice with phosphate buffer saline (PBS) and 20 μL of the MTT [3-(4,5-dimethythiazol-2-yl)-2,5-diphenyltetrazolium bromide] staining solution (5 mgmL^{-1} in phosphate buffer saline) was added to each well and plate was incubated at 37 °C. After 4 h, 100 μL of DMSO was added to each well to dissolve the formazan crystals and absorbance was recorded at 570 nm using micro plate reader [23].

2.3.2 Photocleavage Study of pBR322 DNA

Supercoiled pBR322 DNA (200 ng) in TAE buffer (40 mM Tris-Acetate, 1 mM EDTA) was treated with synthesized ligands and their respective metal (II) complexes to yield a total volume of 10 μL and then incubated in dark for 30 min at 37 °C. Different concentrations of compounds were tested; 30, 40 and 50 μM. The reaction was quenched by the addition of 3 μL loading buffer and then the resulting solutions were loaded on a 2% Agarose gel. Electrophoresis was carried out at 80 V for 1 hr in TAE buffer (pH 8.0). DNA bands were visualized under UV light and photographed [24].

2.3.3 Cell Apoptosis and Fluorescence Imaging

The cells were seeded in a 24-well flat bottom micro plate containing cover slips and maintained at 37 °C in CO_2 incubator overnight and treated with 200 μgmL^{-1} of compound for 48 h. After the incubation, cells were washed with PBS (phosphate buffer saline) and fixed with 4% paraformaldehyde for 30 min. Then, 20 μL of DAPI [4′,6-diamidino-2-phenylindole] was added to the cells, which were incubated for 5 min at room temperature in the dark and images were taken under fluorescent microscope (Olympus BX41 microscope). Randomly selecting the fields in the microscope and counted the number of cells undergone apoptosis and the percentage of apoptotic cells was calculated [25].

3. Results and Discussion

3.1 Spectral Characterization

3.1.1 9-Oxo-9*H*-fluorene-1-carboxylic acid (1): The IR spectrum of 9-oxo-9*H*-fluorene-1-carboxylic acid (spectrum 1) betray two characteristic bands, one due to ν(C=O) group of carboxylic acid at 1668 cm^{-1}, which has shifted to lower frequency due to conjugation with ν(C=C) of fluorenone ring, another sharp absorption band at 1746 cm^{-1} is due to ketone ν(C=O) group vibrations. The sharp medium absorption band is observed at 1279 cm^{-1} infers the presence of C–O linkage in carboxylic acid functional group. The weak absorption bands at 1604 cm^{-1} and 1574 cm^{-1} are attributed to aromatic ν(C=C) vibrations.

The ^{1}H NMR spectrum of 9-oxo-9*H*-fluorene-1-carboxylic acid (spectrum 2) exhibit a broad peak centered at 3.6 ppm due to the proton attached to carboxylic acid group. Remaining protons are aromatic in nature and are resonated between 7.0-9.0 ppm. **^{1}H NMR** (400MHz, DMSO-d_6) δ/ppm: 3.6(br, 1H, –OH), 7.33(t, 1H, J = 7.8 Hz), 7.46(d, 1H, J = 7.6 Hz), 7.56(m, 3H), 7.67(d, 1H, J = 7.6 Hz), 7.76(d, 1H, J = 7.6 Hz).

3.1.2 IR Spectral Studies of Ligands and Their Respective Metal (II) Complexes

To identify the bonding mode as well as the complexation behavior, the IR spectra were recorded for the synthesized hydrazone Schiff base ligands and their respective metal complexes. The IR spectrum of ligand 1 (LH^1) is reproduced in spectrum 3. The sharp intense band at 1698 cm^{-1} is assigned to ν(C=O) of carboxylic acid group. Another sharp band at 1659 cm^{-1} is due to ν(C=O) vibrations of amide group. One more band at 1631 cm^{-1} is due to hydrazone ν(C=N) group. The weak broad bands at 3189 cm^{-1} and 3032 cm^{-1} are due to ν(N–H) and ν(O–H) respectively.

Similar observations are made for ligand 2 (LH^2, spectrum 4) as well, the spectrum exhibit two weak broad bands at 3265 and 3209 cm^{-1} due to phenolic ν(O–H) and carboxylic ν(O–H) vibrations. The sharp intense band at 1675 cm^{-1} is assigned to ν(C=O) of carboxylic acid. Sharp band appearing at 1652 cm^{-1} is due to amide ν(C=O) group vibrations. Hydrazone ν(C=N) group vibrations are seen at 1637 cm^{-1}. The band due to ν (N–H) is masked by the two broad ν(O–H) vibrations in the region 3100-3500 cm^{-1}. The diagnostic IR frequencies of ligands and their copper (II) complexes are compiled in Table 1.

In all the metal (II) complexes the hydrazone ν(C=N) band is shifted to lower wave number, which infers the involvement of nitrogen atom of hydrazone group in coordination to the central metal ion [26]. The absence of broad band in the region 3200-3650 cm^{-1} infers the coordination of carboxylic acid oxygen via deprotonation. Further, the strong band due to ν(C=O) of carboxylic acid group has disappeared upon complex formation, since in carboxylate ion the negative charge is equally distributed on two oxygen atoms due to resonance, thereby decreasing the bond order. This implies that, the carboxylate ion is involved in bond formation [27]. Simultaneously, two new bands have appeared in the range 1580-1610 cm^{-1} and 1360-1380 cm^{-1} which are assigned to the asymmetric and symmetric stretching frequencies of coordinated carboxylate ion respectively. The amide carbonyl stretching frequency ν(C=O) observed at 1659 and 1652 cm^{-1} in LH^1 (spectrum 3) and LH^2 (spectrum 4) respectively have shifted to the lower wave number value of 1628 and 1632 cm^{-1} in $Cu(L^1)_2$ (spectrum 5) and $Cu(L^2)_2$ (spectrum 6) respectively indicating the coordination of amide carbonyl oxygen to the central metal ion. The medium vibrations due to ν (M–O) are observed between 550-600 cm^{-1} [28, 29]. IR data suggests the ONO donor tridentate behavior of the ligands.

Table 1. Prominent infrared frequencies (in cm^{-1}) of ligands (LH^1 and LH^2) and copper (II) complexes.

m = medium, s = strong, br = broad

Compound	ν(C=O)^s Carboxylic acid	ν(C=O)^s Amide	ν(N–H)^{br}	ν(C=N)^s	ν(COO)		Phenolic ν(O–H)^{br}	ν(O–H)^{br} Acidic	ν(M–O)^m
					ν_{asym}	ν_{sym}			
LH^1	1698	1659	3189 & 3163	1631	1602	1306	---	3032	---
$Cu(L^1)_2$	disappeared	1628	3185 & 3159	1600	1590	1373	---	disappeared	559
LH^2	1675	1652	Masked	1637	1606	1323	3265	3209	---
$Cu(L^2)_2$	disappeared	1632	3538 & 3429	1613	1586	1375	3245	disappeared	577

3.1.3 ^{1}H and ^{13}C NMR Spectral Studies

The ^{1}H NMR spectrum of ligand 1 (LH^1, spectrum 7) shows a broad singlet at 15.20 ppm due to the proton attached to carboxylic acid oxygen [30]. Another broad singlet at 12.25 ppm is due to the amido proton (–NH–). Remaining protons are aromatic in nature and appeared as multiplets between 7.0-9.0 ppm. **^{1}H NMR** (400MHz, DMSO-d_6) δ/ppm: 7.69(m, 6H), 8.05(m, 2H), 8.17(m, 4H), 12.25(s, 1H, -NH), 15.20(s, 1H, –OH). ^{13}C NMR spectrum of ligand 1 (LH^1, spectrum 9) shows a characteristic peak due to carboxylic acid carbon at 167 ppm. The peak at 163 ppm is due to the presence of amide carbon. The bridging carbon of fluorene ring is resonating at 155 ppm. Remaining carbon nuclei are part of the aromatic ring and are resonating in the range 120-150 ppm [31].

The ^{1}H NMR spectrum of ligand 2 (LH^2, spectrum 8) shows broad singlets at 15.48, 12.05 and 10.32 ppm due to the proton attached to carboxylic acid oxygen, the amido proton (–NH–) and the phenolic –OH respectively. Aromatic protons appeared as multiplets in the range 6.0-9.0 ppm. **^{1}H NMR** (400MHz, DMSO-d_6) δ/ppm: 6.96(d, 2H, J = 8.36 Hz), 7.57(t, 1H, J = 7.6 Hz), 7.66(m, 2H), 8.02(m, 4H), 8.17(m, 2H), 10.32(br, 1H, Phe-H), 12.02(s, 1H, –NH), 15.48(br, 1H, acidic-H). ^{13}C NMR spectrum of ligand 2 (LH^2, spectrum 10) displays a characteristic peak due to carbon attached to carboxylic acid group at 170 ppm. The peak at 165 ppm is due to the presence of amide carbon. The carbon attached to phenolic –OH is deshielded and is resonating downfield at 161 ppm. The bridging carbon of fluorene ring is resonating at 155 ppm. Remaining carbon nuclei are part of the aromatic ring and are resonating between 110-150 ppm [31].

3.1.4 Mass Spectral Studies

The mass spectral data of ligands 1 (LH^1) and 2 (LH^2) and their copper (II) complexes [$Cu(L^1)_2$ and $Cu(L^2)_2$] are depicted in spectrum 11, 12, 13 and 14 respectively. The ligands LH^1 and LH^2 exhibit $[M]^+$ and $[M+1]^+$ peaks at m/z 342, 359 respectively. The fragmentation peaks at m/z 325 and 341 in LH^1 and LH^2 respectively, are due to the loss of OH radical. Electrospray ionization mass spectral study (ESI-MS) of metal (II) complexes supports 1 : 2 $[(ML)_2]$ stoichiometry. Copper (II) complexes, $Cu(L^1)_2$ and $Cu(L^2)_2$ show $[M+1]^+$ and $[M-1]^+$ peaks at m/z 746 and 776 respectively; which are matching very well with the predicted molecular

weights of the compounds and this confirms the formation of metal (II) complexes in each case [32, 33].

3.1.5 Electronic Spectral Studies

Electronic spectra of ligands 1 (LH^1, spectrum 15) and 2 (LH^2, spectrum 16) were recorded in methanol and their respective metal (II) complexes were recorded in DMF. The free ligands absorb strongly at 348 and 355 nm due to intra ligand $\pi \longrightarrow \pi^*$ transitions. Absorptions at 412, 432 nm (in LH^1) and 415, 440 nm (in LH^2) are attributed to $n \longrightarrow \pi^*$ transitions associated with carbonyl groups and hydrazone (C=N) group. The bathochromic (red) shift is observed in all the cases upon complex formation due to the donation of charge density to the central metal ion for the coordination. This confirms that, the nitrogen atom of hydrazone group, the oxygen of amide and carboxylic acid group are involved in the bond formation with the central metal ion. IR spectra and mass spectral studies of the metal (II) complexes support the observations made from electronic spectral studies [34, 35].

The absorption spectrum of $Cu(L^1)_2$ and $Cu(L^2)_2$ show one broad peak due to d-d transition centered at 726 and 724 nm respectively, assignable to $^2T_{2g} \longleftarrow {}^2E_g$ as is the consequence of distorted octahedral environment around copper (II) ion [36]. Electronic spectra of $Cu(L^1)_2$ and $Cu(L^2)_2$ complexes are reproduced in spectrum 17 and 18 respectively.

Table 2 shows the solution electronic absorption spectral data of ligands and their respective copper (II) complexes. In case of nickel and cobalt complexes d-d transitions are rarely recorded or too small to be observed, since these transitions are Laporte forbidden.

Table 2. Solution electronic absorption spectral data of ligands (LH^1 and LH^2) and their copper (II) complexes.

Compound	λ_{max} in cm^{-1} (nm)	Band assignments	Geometry
LH^1	28,735 (348), 24,272 (412), 23,148 (432)	$\pi \longrightarrow \pi^*$, $n \longrightarrow \pi^*$, $n \longrightarrow \pi^*$	---
$Cu(L^1)_2$	13,774 (726)	$^2T_{2g} \longleftarrow {}^2E_g$	Octahedral
LH^2	28,169 (355), 24,096 (415), 22,727 (440)	$\pi \longrightarrow \pi^*$, $n \longrightarrow \pi^*$, $n \longrightarrow \pi^*$	---
$Cu(L^2)_2$	13,812 (724)	$^2T_{2g} \longleftarrow {}^2E_g$	Octahedral

3.1.6 Thermal Analysis Studies

Thermal behavior of all the metal complexes was studied over a temperature range of 25-1000 °C under nitrogen atmosphere. Thermograms of $Cu(L^1)_2$, $Ni(L^1)_2$ and $Co(L^1)_2$ complexes are reproduced in entry 19 of supporting information. The copper (II) complex is found to be highly stable up to 225 °C. Later on from 255 – 350 °C, the metal complex decomposes in only one significant step; which infers that, only ligand moiety is present in the complex has lost, after which the formation of metal oxide is observed [37]. This result is in line with the IR, electronic spectral and ESI-MS data. Similar plot is observed in case of $Ni(L^1)_2$, $Co(L^1)_2$ and second set of complexes as well. Thus, the thermal data of the metal (II) complexes give no evidence for the presence of any other coordinated moieties like water, chloride, methanol, DMF etc.,

3.1.7 Molar Conductivity Studies

Conductivity measurement of metal complexes in solution state is a powerful tool to ascertain their electrolytic nature. Molar conductivity (Λ_m) of all the metal (II) complexes was measured at 25 °C by preparing mmol solutions in DMF using the conductivity bridge (G* = 1). The values obtained for the metal (II) complexes did not exceed 20 Ω^{-1} cm^2 mol^{-1}. These results confirm that, the metal (II) complexes are non-electrolytic in nature, which is due to the absence of counter ions in their structures [38]. The molar conductivity values have been reproduced in

Table 3 along with the elemental analysis data. The detailed experimental results have been tabulated in Table 4. Molar conductivity studies support the observations made in ESI-MS and thermal studies.

Table 3. Elemental analysis of ligands (LH^1 and LH^2) and their respective metal (II) complexes along with molar conductivity data.

Compound	Empirical formula	M%		C%		H%		N%		Color/ % yield	Molar conductivity value, Λ_m ($\Omega^{-1}cm^2mol^{-1}$)
		Obsd.	Calcd.	Obsd.	Calcd.	Obsd.	Calcd.	Obsd.	Calcd.		
LH^1	$C_{21}H_{14}N_2O_3$	--	--	73.72	73.68	4.18	4.12	8.25	8.18	Yellow/93	--
$Cu(L^1)_2$	$C_{42}H_{26}CuN_4O_6$	8.63	8.52	67.71	67.60	3.60	3.51	7.62	7.51	Green/52	16.3
$Ni(L^1)_2$	$C_{42}H_{26}NiN_4O_6$	8.01	7.92	68.11	68.04	3.62	3.53	7.67	7.56	Yellow/45	12.9
$Co(L^1)_2$	$C_{42}H_{26}CoN_4O_6$	8.04	7.95	68.14	68.02	3.66	3.53	7.59	7.55	Yellow/48	15.1
LH^2	$C_{21}H_{14}N_2O_4$	--	--	70.44	70.39	3.99	3.94	7.88	7.82	Yellow/90	--
$Cu(L^2)_2$	$C_{42}H_{26}CuN_4O_8$	8.29	8.17	64.93	64.82	3.49	3.37	7.31	7.20	Brown/58	19.5
$Ni(L^2)_2$	$C_{42}H_{26}NiN_4O_8$	7.67	7.59	64.31	65.23	3.50	3.39	7.33	7.24	Yellow/42	13.6
$Co(L^2)_2$	$C_{42}H_{26}CoN_4O_8$	7.77	7.62	65.34	65.21	3.48	3.39	7.35	7.24	Brownish yellow/50	16.0

Table 4. Molar conductivity (Λ_m) data of synthesized metal (II) complexes.

Complexes	Conductance (G) at 25 °C	Conductivity (κ) in $\mu\Omega^{-1}$	Molar conductivity (Λ_m) in $\Omega^{-1}cm^2mol^{-1}$
		$\kappa = G$ ($\because G^*=1.0$)	$\Lambda_m = (1000\ \kappa)/c$
$Cu(L^1)_2$	16.3 x 10^{-6}	16.3 x 10^{-6}	16.3
$Ni(L^1)_2$	12.9 x 10^{-6}	12.9 x 10^{-6}	12.9
$Co(L^1)_2$	15.1 x 10^{-6}	15.1 x 10^{-6}	15.1
$Cu(L^2)_2$	19.5 x 10^{-6}	19.5 x 10^{-6}	19.5
$Ni(L^2)_2$	13.6 x 10^{-6}	13.6 x 10^{-6}	13.6
$Co(L^2)_2$	16.0 x 10^{-6}	16.0 x 10^{-6}	16.0

Cell constant (G*) of *ELICO CM 180* conductivity meter = 1.0.

Conductance (G) values are obtained from the experiment in $\mu\Omega^{-1}$ or μS.

1mM solutions of metal (II) complexes are prepared in DMF and their conductance (G) is recorded.

3.2 Bioassay Results

3.2.1 Cytotoxicity- *in vitro* Studies

In order to find out the potency and effectiveness of the synthesized compounds as chemotherapeutic drugs, it is important to evaluate the anticancer activity using MTT assay. The *in vitro* anticancer activity of ligands and their metal (II) complexes against A549 and MCF-7 cell lines have been tested by MTT [3-(4,5-dimethylthiazol-2-yl)-2,5-diphenyltetrazolium Bromide] assay, using the untreated cells as control (NC). Ligands and all the metal (II) complexes exhibit concentration-dependent anticancer activity which is evident from the bar plot 1 and 2 (Tables 5 and 6). Each entry in the plot is the mean of triplicate results obtained by carrying out separate experiments. Results are expressed as mean± standard deviation (n = 3). At 5 μM concentration all the compounds show highest cell survival when compared to that at higher concentrations [39-41].

Table 5. Cell viability data of ligands LH^1, LH^2 and six metal (II) complexes for A549 cell line at six different concentrations.

	A549							
Concentration in μgmL^{-1}	**LH^1**	**$Co(L^1)_2$**	**$Cu(L^1)_2$**	**$Ni(L^1)_2$**	**LH^2**	**$Co(L^2)_2$**	**$Cu(L^2)_2$**	**$Ni(L^2)_2$**
5	98.36±0.1643	94.85±0.1715	96.67±0.2694	95.49±0.2876	97.60±0.3226	91.41±0.3171	88.84±0.4009	92.48±0.3151
10	92.43±0.2017	87.34±0.5530	90.48±0.2041	89.42±0.2465	91.52±0.2641	84.37±0.2947	77.24±0.1685	88.39±0.2369
20	80.48±0.2379	78.47±0.3054	81.60±0.2166	73.52±0.2524	81.59±0.1902	77.60±0.2046	67.43±0.3844	78.50±0.2046
30	66.75±0.1515	73.48±0.2449	53.93±0.2120	67.26±0.2597	53.39±0.2120	70.36±0.2531	52.44±0.2416	67.63±0.3260
40	61.24±0.1574	54.96±0.2089	43.36±0.2206	59.48±9.2169	43.36±0.2206	47.49±0.3542	32.58±0.3193	56.45±0.3127
50	54.37±0.1968	44.71±0.5213	36.45±0.2293	48.30±0.1470	36.45±0.2293	44.53±0.2562	22.43±0.3785	50.39±0.3111

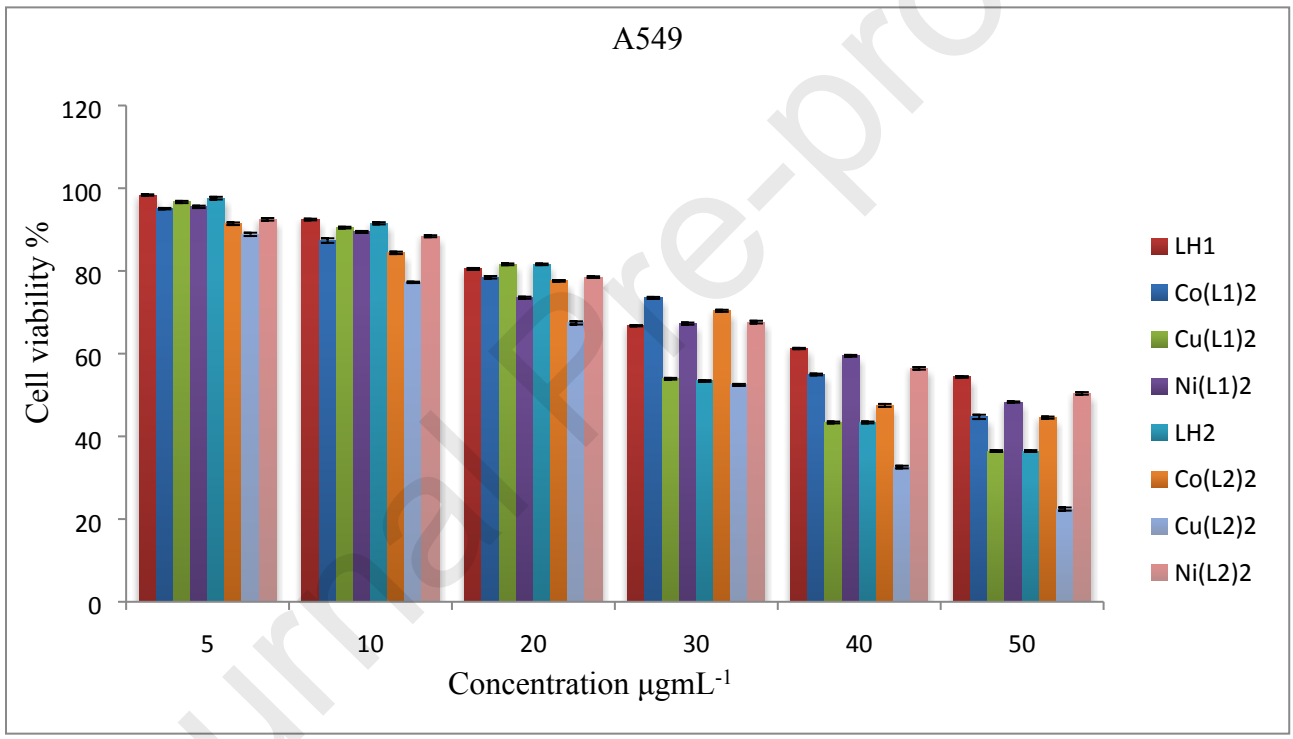

Plot 1. Bar graph showing the % cell viability of ligands and their metal (II) complexes for A549 cell line v/s concentration in μgmL^{-1}.

Table 6. Cell viability data of ligands LH^1, LH^2 and six metal (II) complexes for MCF-7 cell line at six different concentrations.

	MCF-7							
Concentration in µgmL^{-1}	**LH^1**	**$Co(L^1)_2$**	**$Cu(L^1)_2$**	**$Ni(L^1)_2$**	**LH^2**	**$Co(L^2)_2$**	**$Cu(L^2)_2$**	**$Ni(L^2)_2$**
5	97.40±0.3559	98.78±0.2904	88.49±0.2248	86.43±0.3007	64.51±0.3353	72.52±0.0623	66.59±0.3950	89.65±0.2658
10	88.46±0.3374	96.28±0.1557	66.35±0.2458	77.34±0.2458	59.53±0.2455	61.29±0.1498	56.36±0.2795	84.44±0.1948
20	81.56±0.3026	91.62±0.2135	60.40±0.2763	74.45±0.2782	56.35±0.1498	59.54±0.1883	34.57±0.2169	80.52±0.3408
30	77.39±0.2223	66.47±0.2409	57.44±0.1899	70.32±0.2416	50.50±0.2458	51.82±0.0980	32.36±0.2740	77.30±0.1569
40	65.26±0.1146	56.58±0.2164	56.39±0.2583	65.45±0.1730	45.41±0.0492	46.43±0.3182	30.84±0.1271	71.34±0.1586
50	57.42±0.3627	48.61±0.3704	51.34±0.1407	56.39±0.2583	41.68±0.1818	35.48±0.1552	29.34±0.1186	56.31±0.1236

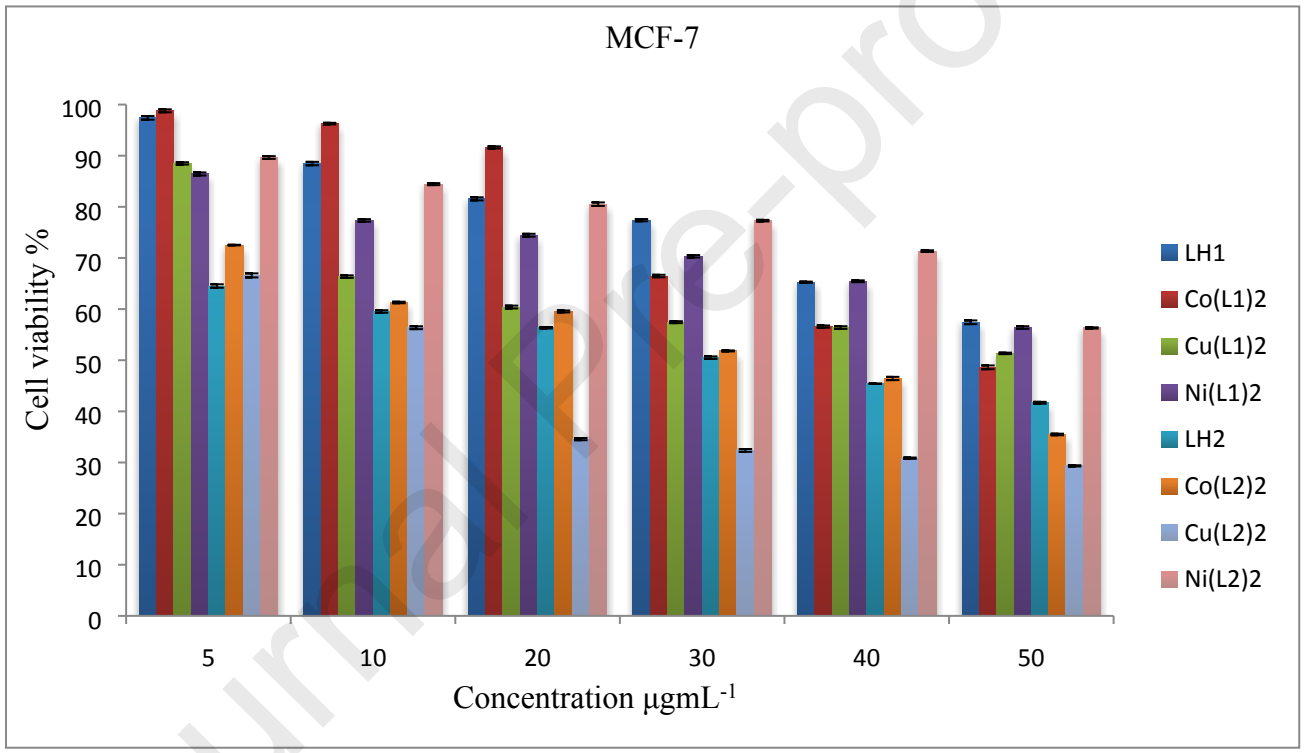

Plot 2. Bar graph showing % cell viability of ligands and their metal (II) complexes for MCF-7 cell line v/s concentration in µgmL^{-1}.

The % cell viability (% cell survival) of the cells is calculated using the relation,

% Viability = (Mean OD of test compound/Mean OD of negative control) x 100

Inhibiting cells (%) =100 - Surviving cells.

The IC50 was extrapolated from the dose-response curve. The drug concentration that reduced the viability of cells by 50% (IC50) was determined by plotting triplicate data points over a concentration range and calculating the values using *GraphPad Prism Ver. 5.1* program. The IC50 (Half maximal inhibitory concentration) values of ligands and their metal (II) complexes suggest that synthesized compounds are more active towards A549 cell line when compared with the standard drug Paclitaxel. In case of MCF-7 cell line, compound $Cu(L^2)_2$ is found to be more active than the standard drug Paclitaxel. Further, activity of the metal (II) complexes is more compared to that of free ligands which is evident from their lower IC50 values. IC50 values of ligands and their respective metal (II) complexes in μgmL^{-1} for both the cell lines tested are compiled in Table 7. The cell images of anticancer activity are reproduced in Fig. 1 (LH^1 and its metal (II) complexes) and Fig. 2 (LH^2 and its metal (II) complexes). The results obtained from these images confirm apoptosis induced in cancer cells (characterized by distorted cytoplasm, compactness of cancer cells, ruptured cell walls) when treated with ligands and their metal (II) complexes; it is found to be more effective when compared with that of standard drug Paclitaxel [42-44].

Table 7. IC50 values of ligands and their respective metal (II) complexes in μgmL^{-1} for A549 and MCF-7 cell lines tested.

Compound	Cell line	
	A549 (μgmL^{-1})	MCF-7 (μgmL^{-1})
LH^1	54.740	66.950
$Co(L^1)_2$	47.390	46.380
$Cu(L^1)_2$	35.560	52.010
$Ni(L^1)_2$	50.330	99.510
LH^2	56.610	27.580
$Co(L^2)_2$	44.140	27.870
$Cu(L^2)_2$	27.220	10.940
$Ni(L^2)_2$	51.040	92.610
Paclitaxel	**73.25**	**23.476**

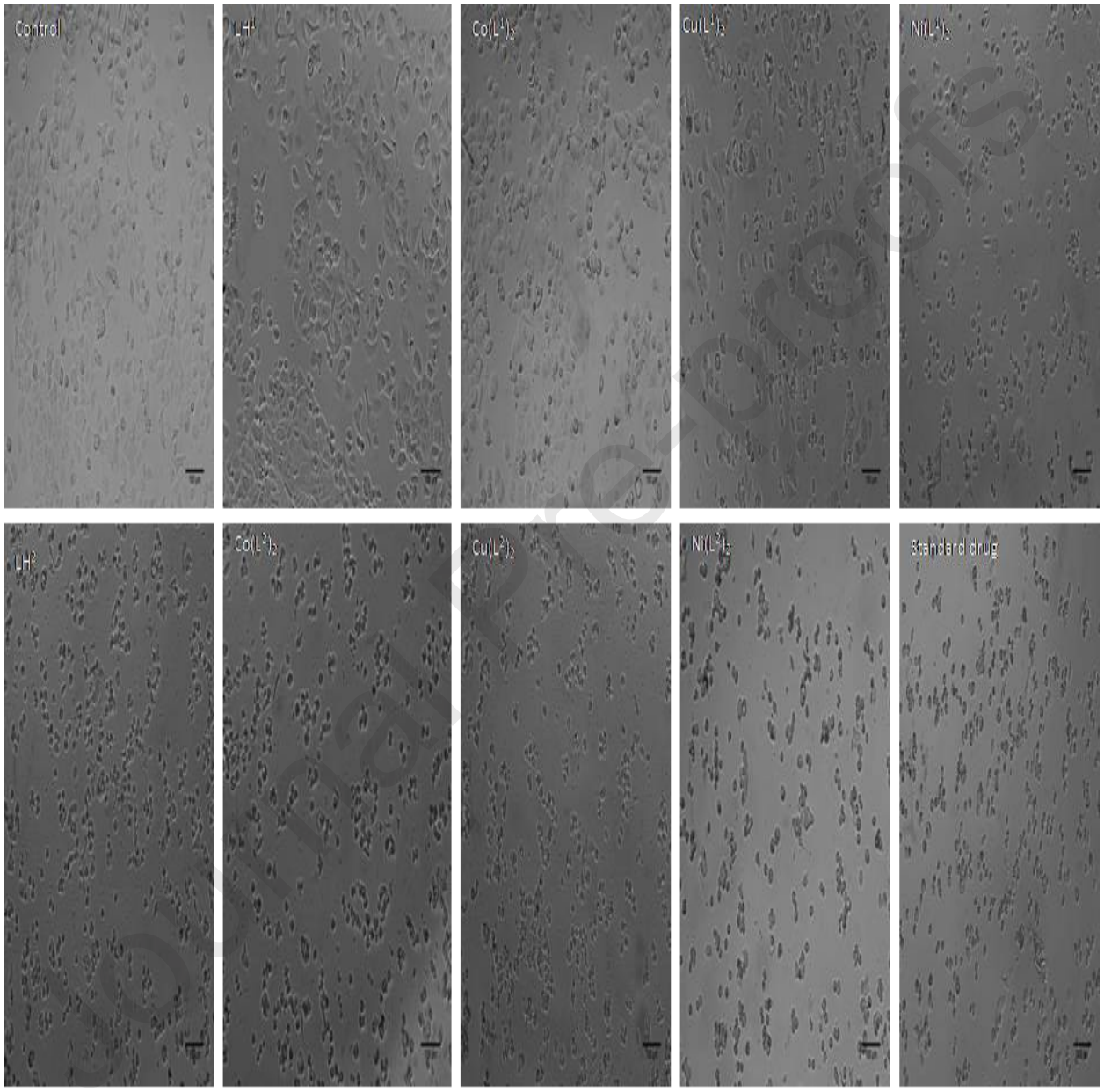

MTT images of LH^1, LH^2 and six metal (II) complexes for A549 cell line at 50 $\mu g mL^{-1}$

Fig. 1. *In vitro* anticancer activity of ligands LH^1, LH^2 and six metal (II) complexes for A549 cell line.

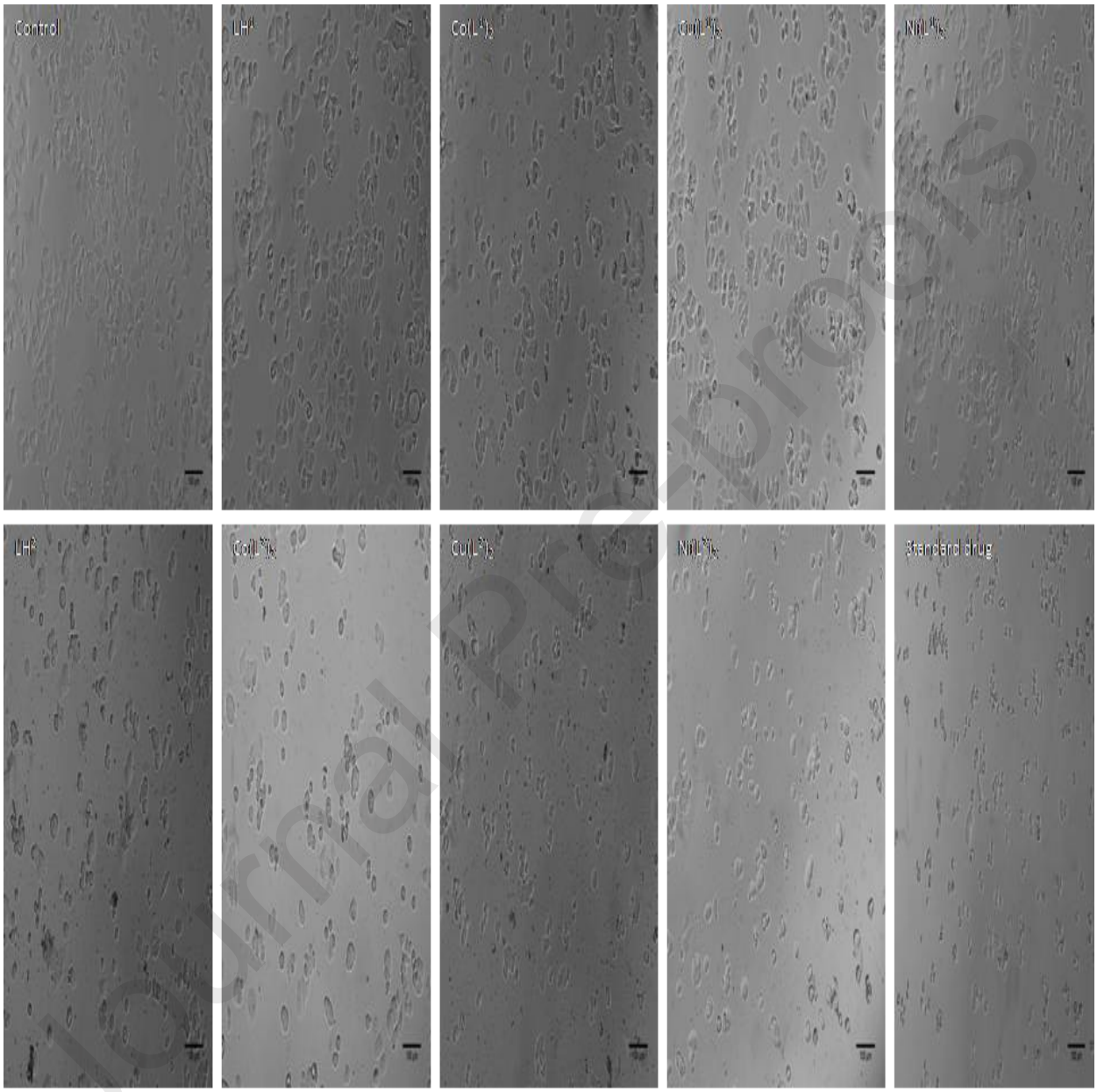

MTT images of LH^1, LH^2 and six metal (II) complexes for MCF 7 cell line at 50 μgmL^{-1}

Fig. 2. *In vitro* anticancer activity of ligands LH^1, LH^2 and six metal (II) complexes for MCF-7 cell line.

3.2.2 DNA Cleavage Studies

Designing small molecules help in targeting specific sites on a DNA strand and can lead to novel therapeutic agents. Photo cleavage study of DNA also helps in various applications like photodynamic therapy of cancers, DNA foot printing agents and in genomic research [45-47]. The ligand and their metal (II) complexes were tested at different concentrations (5, 10, 20, 40, 50 μM) to evaluate their cleaving ability. They displayed DNA degradation effect which verifies their binding affinity to the supercoiled pBR322 DNA. The synthesized metal (II) complexes exhibited the enhanced cleavage compared to free ligands (LH^1 and LH^2) [48, 49]. The DNA cleavage images are reproduced in Fig. 3.

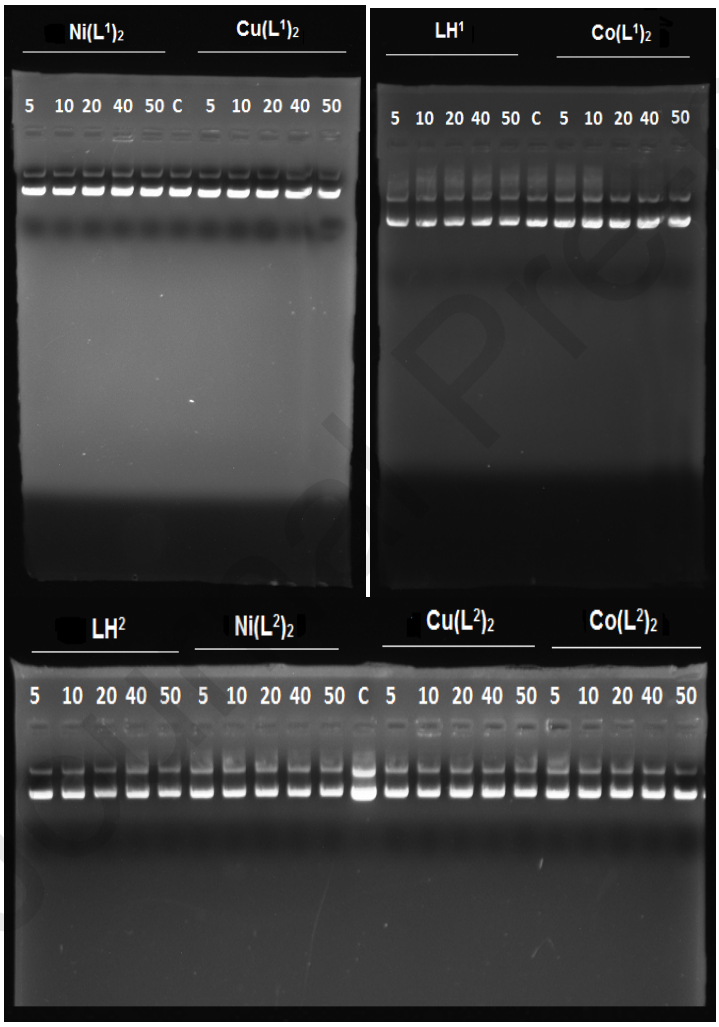

Fig. 3. Gel electrophoresis images of ligands 1 and 2 (LH^1 and LH^2) and their respective metal (II) complexes showing the effect on pBR322 DNA compared with negative control.

3.2.3 Cell Morphology Studies by Fluorescence Microscopy

DAPI [4′,6-diamidino-2-phenylindole] is a fluorescent dye; a DNA specific probe which enhances the fluorescence and forms a complex with DNA by preferentially binding to the Adenine-Thymine (A-T) regions of double stranded DNA. The fluorescence enhancement is particularly good for mitochondrial DNA which is rich in A-T sequences. DAPI is a DNA specific fluorescent stain and it is not sensitive to RNA. The fluorescence enhancement of DAPI in the presence of DNA is the basis for a simple and rapid method for DNA microassay in the presence of RNA, proteins and cellular homogenates [50]. This technique is employed in studying the cell apoptosis induced by the synthesized ligands and their respective metal (II) complexes, by staining the 'cell treated' and 'untreated (NC)' with DAPI. The cell death was characterized by shrinkage of cell walls, nuclear fragmentation and DNA condensation [51-54]. These results confirm the inference made in case of MTT assay. The fluorescence images are reproduced in Figs. 4 and 5.

Cells treated: Cancer cells treated with synthesized ligands and their respective metal (II) complexes.

Untreated cells: Cancer cells untreated with synthesized compounds are used as negative control (NC).

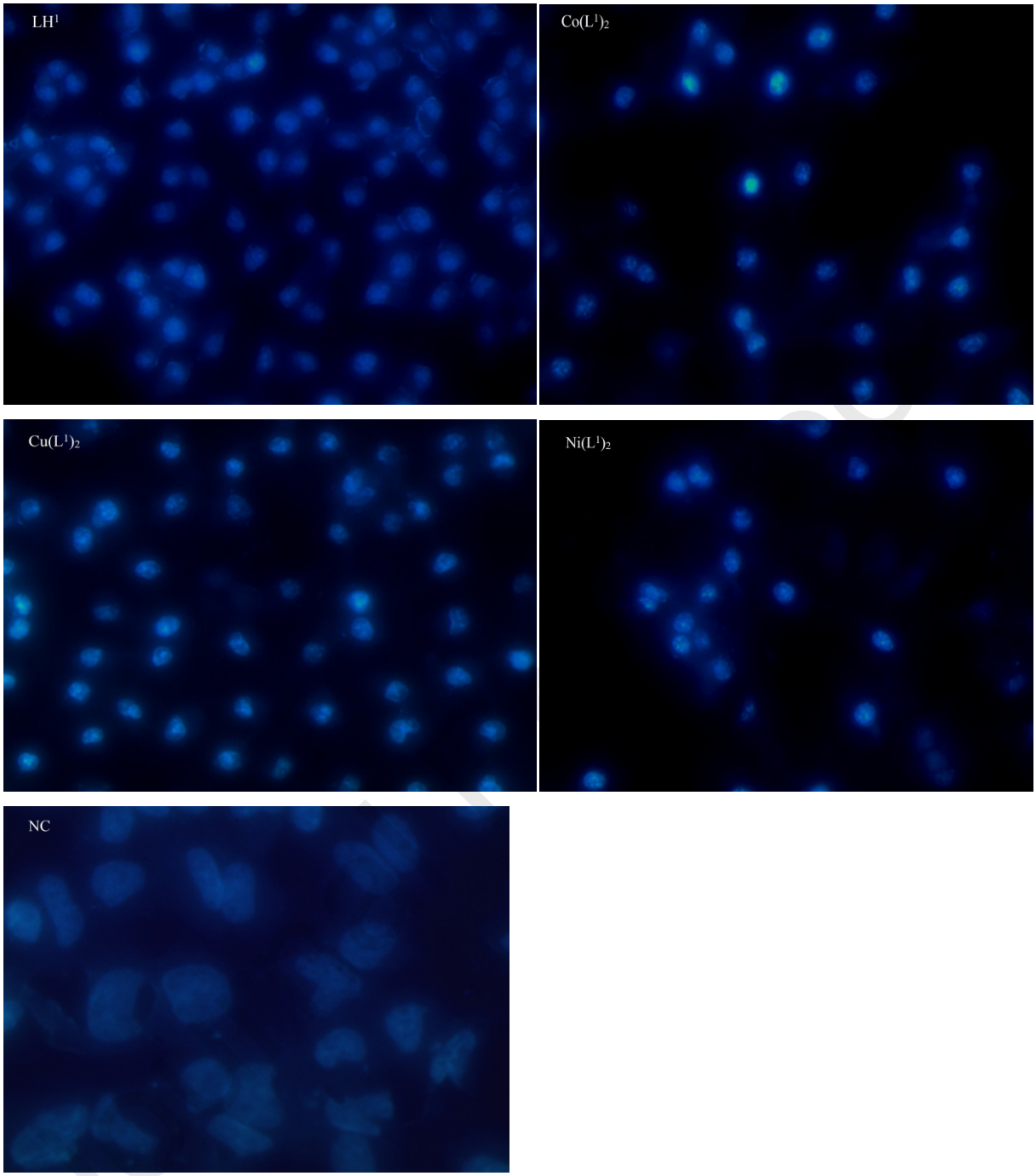

Fig. 4. Fluorescence microscopy images of cells stained with DAPI, showing untreated control cells (NC) and cells treated with ligand 1 (LH^1) and its metal (II) complexes.

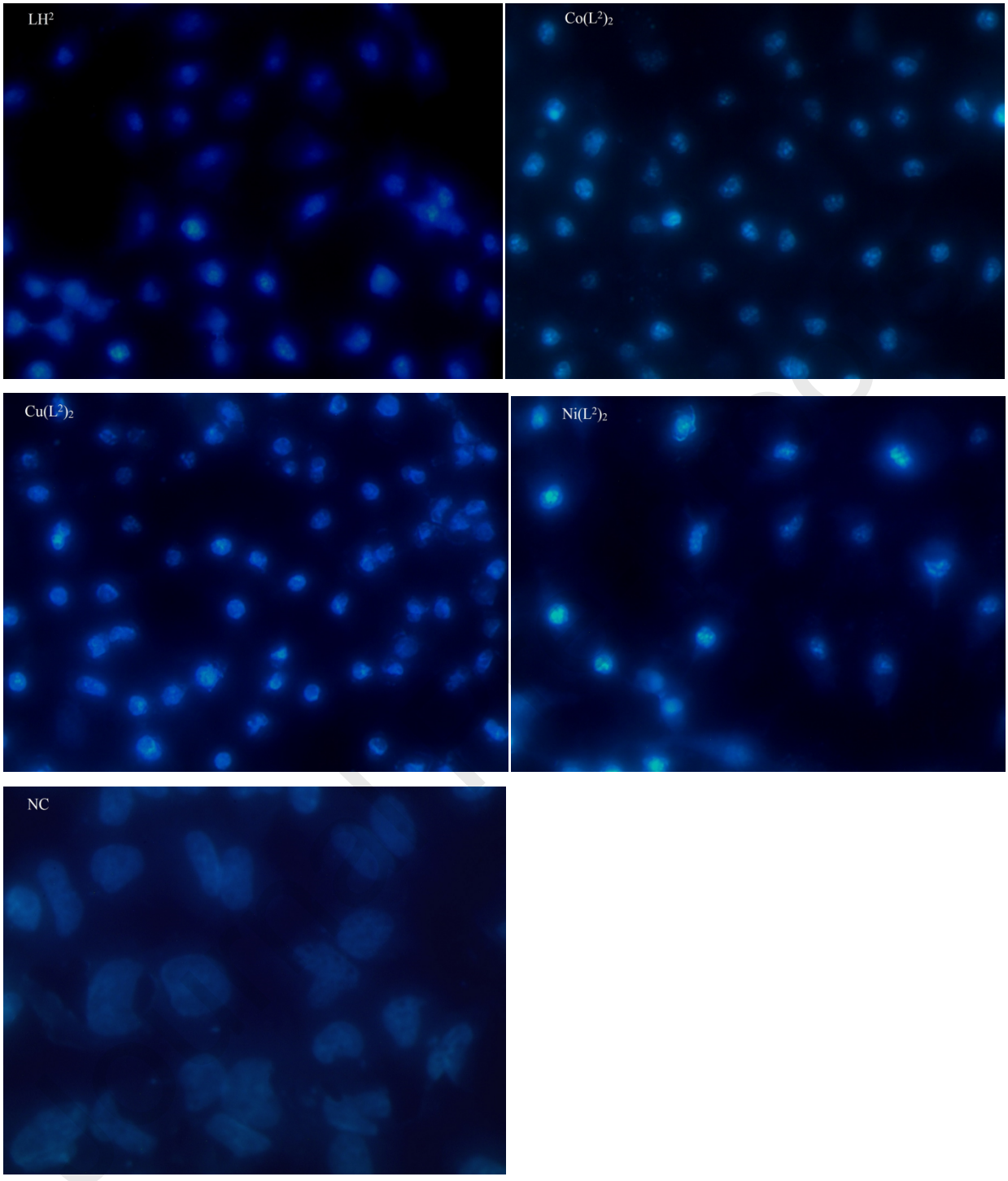

Fig. 5. Fluorescence microscopy images of cells stained with DAPI, showing untreated control cells (NC) and cells treated with ligand 2 (LH^2) and its metal (II) complexes.

4. Conclusions

In the current study two new ligands were synthesized; the key precursors, ligands and their transition metal (II) complexes were characterized by spectral (^{1}H, ^{13}C NMR, IR, GC-MS, electronic), elemental analysis, thermal and molar conductivity measurements. The ligands and their transition metal (II) complexes were screened for DNA cleavage, fluorescence imaging using DAPI staining, anticancer activity with apoptotic effect. The hydrazone Schiff bases and their metal (II) complexes successfully cleaved the pBR322 DNA. Cell apoptosis is confirmed by the fluorescence images obtained upon treatment of cancer cells (A549 and MCF-7) with the synthesized compounds. Concentration-dependent cell survival rate was observed during *in vitro* anticancer activity, which decreases with increase in concentration. The IC50 values of ligands and their metal (II) complexes suggest that synthesized compounds are more active towards A549 cell line when compared with the standard drug Paclitaxel. In case of MCF-7 cell line, compound $Cu(L^2)_2$ is found to be more active than the standard drug Paclitaxel.

Acknowledgements

The author acknowledges University Grants Commission, New Delhi, India, for providing the financial support through *BSR-RFSMS* fellowship [F. NO: 25-1/2014-15(BSR)/7-100/2007/(BSR) Dated: 05/11/2015]. Authors are grateful to the Chairman, Department of Chemistry, Karnatak University Dharwad, for providing the laboratory facilities. Authors are thankful to University Scientific Instrumentation Centre (USIC) and SAIF K. U. D, SAIF IIT Madras and IISC Bangaluru, for providing instrumental facilities. The authors also express their gratitude to Maratha Mandal's Central Research Laboratory Belagavi, Karnataka, India, for their valuable support for bioassay related study.

Disclosure Statement

Authors do not have any conflicts of interest to declare.

References

1. C. Everett Koop. *Am. J. Public Health.* 96 (2006) 2090-2092.
2. IARC. *Cancer Incidence and Mortality Worldwide*; International Agency for Research on Cancer: Lyon, France, 2011.
3. WHO. *Global Status Report on Non-communicable Diseases 2010*; WHO: Geneva, Switzerland, (2011) 11–15.
4. Global cancer facts and figures by American cancer society; https://www.cancer.org/research/cancer-facts-statistics/global.html (accessed 19 September 2019).
5. W. You, M. Henneberg. *Evol. Appl.* 11 (2018) 140-152. DOI: 10.1111/eva.12523.
6. American society of clinical oncology; https://www.cancer.net/navigating-cancer-care/cancer-basics/what-cancer (accessed 19 September 2019).
7. National Center for Biotechnology Information, U. S. National Library of Medicine. https://www.ncbi.nlm.nih.gov/books/NBK9963/ (accessed 19 September 2019).
8. F. Keil, E. Selzer, A. Berghold, S. Reinisch, K. S. Kapp, A. De Vries, R. Greil, B. Bachtiary, C. Tinchon, W. Anderhuber, M. Burian, A. K. Kasparek, W. Elsäßer, H. Kainz, R. Riedl, M. Kopp, G. Kornek. *Eur. J. Cancer.* 49 (2013) 352−359. DOI: 10.1016/j.ejca.2012.08.004.
9. S. Jain, J. Dwivedi, P. K. Jain, S. Satpathy, A. Patra. *Pharmacogn. J.* 8 (2016) 87-102. DOI: 10.5530/pj.2016.2.1.
10. National Cancer Institute. U. S. Department of Health and Human Services. https://www.cancer.gov/about-cancer/treatment/side-effects (accessed 19 September 2019).
11. K. D. Mjos, C. Orvig. *Chem. Rev.* 114 (2014) 4540-4563. DOI: 10.1021/cr400460s.
12. S. Quaresma, V. André, A. Fernandes, M. T. Duarte. *Inorganica Chim. Acta.* 455 (2017) 309-318. DOI: 10.1016/j.ica.2016.09.033.
13. S. Ishak, G. Y. Yeap, Shanmugapriya, S. Sasidharan, M. M Ito. *J. Mol. Struct.* 1175 (2019) 763-768. DOI: 10.1016/j.molstruc.2018.08.030.
14. F. F. Becker, B. K. Banik. *Front. Chem.* 2 (2014) article 55. DOI: 10.3389/fchem.2014.00055.
15. P. C. Ting, J. F. Lee, M. M. Albanese, W. C. Tom, D. M. Solomon, R. Aslanian, N. Y. Shih, R. West. *Bioorg. Med. Chem. Lett.* 12 (2002) 2643-2646. DOI: 10.1016/S0960-894X(02)00521-8.

16. W. Zeng, T. E. Ballard, A. G. Tkachenko, V. A. Burns, D. L. Feldheim, C. Melande. *Bioorg. Med. Chem. Lett.* 16 (2006) 5148-5151. DOI: 10.1016/j.bmcl.2006.07.024.
17. S. Alcaro, A. Artese, J. N. Iley, R. Maccari, S. Missailidis, F. Ortuso, R. Ottana`, P. Ragazzon, M. G. Vigorit. *Bioorg. Med. Chem. Lett.* 17 (2007) 2509-2514. DOI: 10.1016/j.bmcl.2007.02.022.
18. W. Kemnitzer, N. Sirisoma, B. Nguyen, S. Jiang, S. Kasibhatla, C. C. Grundy, B. Tseng, J. Drewe, S. X. Cai. *Bioorg. Med. Chem. Lett.* 19 (2009) 3045-3049. DOI: 10.1016/j.bmcl.2009.04.009.
19. W. Kemnitzer, N. Sirisoma, S. Jiang, S. Kasibhatla, C. C. Grundy, B. Tseng, J. Drewe, S. X. Cai. *Bioorg. Med. Chem. Lett.* 20 (2010) 1288-1292. DOI: 10.1016/j.bmcl.2009.11.025.
20. T. Leepasert, M. Shahabi, K. Shanab, E. Schirmer, W. Holzer, H. Spreitzer, B. Aicher, G. Müller, E. Günther. *Bioorg. Med. Chem. Lett.* 23 (2013) 5264-5266. DOI: 10.1016/j.bmcl.2013.08.021.
21. M. Kumbar, S. A. Patil, S. M. Kinnal, S. S. Jawoor, A. Shettar. *Chem. Data Collect.* 21 (2019) 100226. DOI: 10.1016/j.cdc.2019.100226.
22. S. A. Patil, V. H. Naik, A. D. Kulkarni, U. Kamble, G. B. Bagihalli, P. S. Badami. *J. Coord. Chem.* 63 (2010) 688-699. DOI: 10.1080/00958971003602269.
23. T. Mosmann. *J. Immun. Methods.* 65 (1983) 55-63. DOI: 10.1016/0022-1759(83)90303-4.
24. T. A. Brown. *Essential Molecular Biology – A Practical Approach*, Vol. 1, 2nd Edn, Oxford University Press, New York (1990).
25. S. S. Bhat, V. K. Revankar, A. Khan, R. J. Butcher, K. Thatipamula. *New J. Chem.* 39 (2015) 3646-3657. DOI: 10.1039/c4nj02394c.
26. K. Nakamoto, *Infrared and Raman Spectra of Inorganic and Coordination Compounds Part A: Theory and Applications in Inorganic Chemistry*, John Wiley & Sons Inc., Hoboken, NJ (2009).
27. G. B. Deacon, R. J. Phillips. *Coord. Chem. Rev.* 33 (1980) 227-250. DOI: 10.1016/S0010-8545(00)80455-5.
28. L. J. Bellamy. The Infrared Spectra of Complex Molecules, Methuen, London, 353 (1958).
29. D. Hegde, S. Dodamani, V. Kumbar, S. Jalalpure, K. B. Gudasi. *Appl. Organomet. Chem.* 31 (2017) p. e3851. DOI: 10.1002/aoc.3851.

30. S. A. Patil, C. T. Prabhakara, B. M. Halasangi, S. S. Toragalmath, P. S. Badami. *Spectrochim. Acta A Mol. Biomol. Spectrosc.* 137 (2015) 641-651. DOI: 10.1016/j.saa.2014.08.028.
31. Donald L. Pavia, Gary M. Lampman, George S. Kriz. *Introduction to Spectroscopy,* 3rd edn.
32. Edmond de Hoffmann and Vincent Stroobant. Mass Spectrometry, Principles and Applications, 3rd edn, John Wiley and Sons.
33. Jurgen H. Gross. Mass Spectrometry, A Textbook. 2nd edn, Springer Publications.
34. John R. Ferraro. Low Frequency Vibrations of Inorganic and Coordination Compounds, *Plenum Press*, New York (1971).
35. L. Antolini, L. Menabue, G. C. Pellacani, M. Saladini, L. P. Battaglia, A. B. Corradi, G. Marcotrigiano. *J. Chem. Soc. Dalton Trans.* 10 (1984) 2325-2326. DOI: 10.1039/DT9840002325.
36. A. B. P. Lever. *Inorganic Electronic Spectroscopy*, Elsevier Publishing Company, Amsterdam (1968).
37. C. T. Prabhakara, S. A. Patil, A. D. Kulkarni, V. H. Naik, M. Manjunatha, S. M. Kinnal, P. S. Badami. *J. Photochem. Photobiol. B, Biol.* 148 (2015) 322-332. DOI: 10.1016/j.jphotobiol.2015.03.033.
38. W. J. Geary. *Coord. Chem. Rev*. 7 (1971) 81-122. DOI: 10.1016/S0010-8545(00)80009-0.
39. Q. Guo, S. Liu, Q. Liu, H. Xu, J. Zhao, H. Wu, X. Li, J. Wang. *J. Coord. Chem.* 65 (2012) 1781-1791. DOI: 10.1080/00958972.2012.680592.
40. S. S. Jawoor, S. A. Patil, S. S. Toragalmath. *J. Coord. Chem.* 71 (2018) 271-283. DOI: 10.1080/00958972.2017.1421951.
41. P. R. Reddy, M. K. Swamy, B. Satyanarayana. *Chem. Data Collect.* 17-18 (2018) 419-430. DOI: 10.1016/j.cdc.2018.11.001.
42. P. J. Raj, D. Bahulayan. *Tetrahedron Lett.* 58 (2017) 2122-2126. DOI: 10.1016/j.tetlet.2017.04.052.
43. Z. Saedi, E. Hoveizi, M. Roushani, S. Massahi, M. Hadian, K. Salehi. *J. Mol. Struct.* 1176 (2019) 207-216. DOI: 10.1016/j.molstruc.2018.08.072.
44. P. Krishnamoorthy, P. Sathyadevi, A. H. Cowley, R. R. Butorac, N. Dharmaraj. *Eur. J. Med. Chem.* 46 (2011) 3376-3387. DOI: 10.1016/j.ejmech.2011.05.001.

45. C. X. Zhang, S. J. Lippard. *Curr. Opin. Chem. Biol.* 7 (2003) 481-489. DOI: 10.1016/S1367-5931(03)00081-4.
46. C. J. Burrows, J. G. Muller. *Chem. Rev.* 98 (1998) 1109-1151. DOI: 10.1021/cr960421s.
47. S. Murali, C. V. Sastri, B. G. Maiya. *Proc. Indian Acad. Sci. (Chem. Sci)*. 114 (2002) 403-415. https://www.ias.ac.in/article/fulltext/jcsc/114/04/0403-0415.
48. J. Yuan, K. Wei, G. Zhang, N. Chen, X. Wei, C. Pan, D. Mo, G. Su. *Eur. J. Med. Chem.* 169 (2019) 144-158. DOI: 10.1016/j.ejmech.2019.02.072.
49. D. S. Reddy, M. Kongot, S. P. Netalkar, M. M. Kurjogi, R. Kumar, F. Avecilla, A. Kumar. *Eur. J. Med. Chem.* 150 (2018) 864-875. DOI: 10.1016/j.ejmech.2018.03.042.
50. Jan Kapuscinski. *Biotech. & Histochem.* 70 (1995) 220-233. DOI: 10.3109/10520299509108199.
51. S. S. Bhat, V. K. Revankar, V. Kumbar, K. Bhat, V. A. Kawade. *Acta Cryst.* C74 (2018) 146-151. DOI: 10.1107/S2053229617018551.
52. A. A. Farahat, A. Kumar, M. Say, T. Wenzler, R. Brun, A. Paul, W. D. Wilson, D. W. Boykin. *Eur. J. Med. Chem.* 128 (2017) 70-78. DOI: 10.1016/j.ejmech.2017.01.037.
53. M. K. Ghosh, S. Mandal, S. Mohapatra, A. Chatterjee, A. Bhattacharyya, S. Chattopadhyay. *J. Coord. Chem.* 72 (2019) 180-200. DOI: 10.1080/00958972.2018.1550256.
54. S. S. Bhat, N. Shivalingegowda, V. K. Revankar, N. K. Lokanath, M. S. Kugaji, V. Kumbar, K. Bhat. *J. Inorg. Biochem.* 177 (2017) 127-137. DOI: 10.1016/j.jinorgbio.2017.09.020.

Author Agreement:

All authors have seen the final version of the manuscript and whole heartedly approved the same before submission.

Conflict of Interest:

Authors do not have any conflicts of interest to declare.

Disclosure Statement

There is no financial/personal interest that could affect our objectivity.

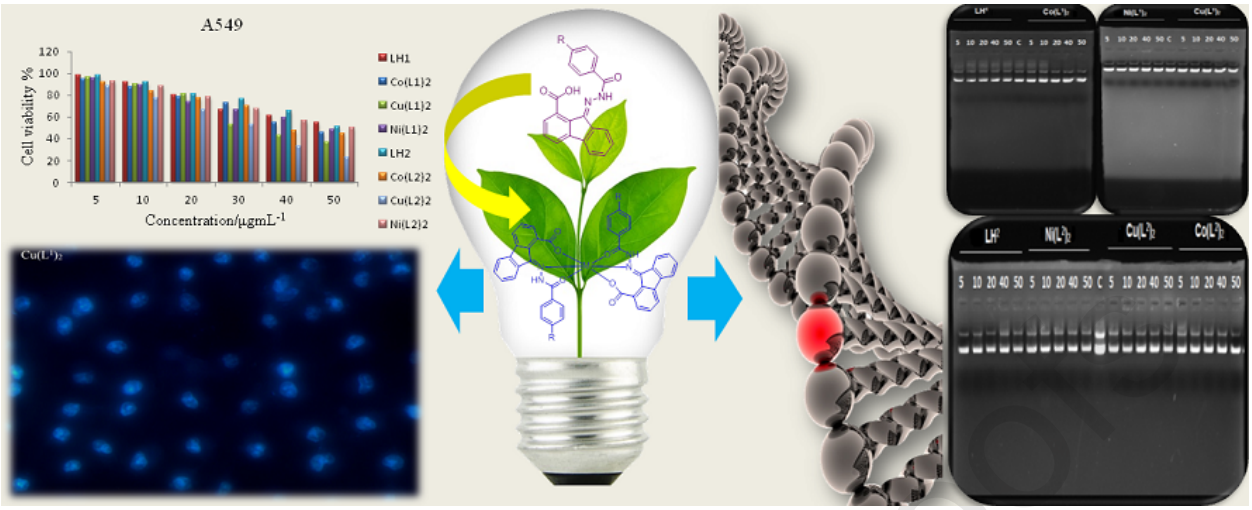

Highlights

- The manuscript describes the synthesis of two new hydrazone Schiff base ligands.
- Synthesis of metal complexes from greener protocol.
- Structure of synthesized compounds was confirmed by analytical and spectroscopic methods.
- DNA cleavage, DAPI staining and anticancer activity studies were carried out.

Study confirms that, synthesized compounds are more active towards A549 cell line when compared to that of standard drug Paclitaxel.